Ukrainian Journal of Physical Optics
ISSUE 3
2026

PECULIARITIES OF HOT CARRIER TRANSPORT ACROSS GAAS *P-N* JUNCTIONS UNDER INTERBAND AND INTRABAND EXCITATION

O. MASALSKYI [1,2], I. ZHARCHENKO [1,2], AND J. GRADAUSKAS [2]

[1] State Research Institute Center for Physical Sciences and Technology, Saulėtekio Avenue 3, 10257, Vilnius, Lithuania
[2] Vilnius Gediminas Technical University, Saulėtekio Avenue 11, 10223 Vilnius, Lithuania
* Corresponding author: oleksandr.masalskyi@ftmc.lt

Received: 23.06.2026

Abstract. In photovoltaics, the role of hot carriers is still ambiguous. Their positive role is foreseen in the potential for efficient hot carrier solar cells, while the negative one is considered only as the source of fundamental thermalization losses. In this study, hot carrier photocurrent formation was investigated in a crystalline GaAs *p-n* junction, which is a promising candidate for high-efficiency solar cells, under pulsed laser excitation at 0.532 μm and 1.064 μm. Time-resolved photocurrent measurements were performed at 300 K and 80 K temperatures. Hot carrier photocurrent, with polarity opposite to the electron-hole pair generation-induced current, arises in both cases, i.e., independently of photon energy, but is more pronounced under above-bandgap excitation due to much stronger interband absorption. It is shown that the effective hot carrier temperature, estimated using the temperature-coefficient model, is more effectively raised by above-bandgap radiation at lower sample temperatures.

Keywords: GaAs, hot carriers, temperature coefficient, effective carrier temperature, *p-n* junction, lasers
UDC: 535.215, 621.383.5
DOI: 10.3116/16091833/Ukr.J.Phys.Opt.2026.03225

1. Introduction

The continuous effort to reduce the gap between the theoretically predicted and practically achieved power conversion efficiency of single-junction solar cells requires a detailed understanding of fundamental loss mechanisms. In the classical description according to the Shockley-Queisser (S-Q) theory [1], photons with energy below the semiconductor bandgap are not absorbed, while photons with energy above the bandgap generate electron-hole pairs, and the excess energy is rapidly dissipated to the lattice through carrier thermalization. These below-bandgap and thermalization losses are major intrinsic losses that set the S-Q limit for conventional single-junction solar cells [2].

Hot carriers (HCs) are carriers with kinetic energy exceeding the thermal energy at the crystal lattice temperature [3]. They can be produced in a semiconductor by two principal mechanisms [4-6]. Under above-bandgap excitation (or interband absorption), the excess photon energy remaining after electron-hole pair generation heats the free carriers (FCs). [5,6]. When photons with energies below the bandgap are absorbed (intraband absorption), they heat FCs as well. [4-6]. In both cases, these non-equilibrium carriers have short lifetimes because carrier-carrier and carrier-phonon scattering typically lead to energy relaxation on the femtosecond-to-picosecond timescale [7,8]. Moreover, it was demonstrated that all solar photons contribute to carrier heating, except for photons with energy equal to the bandgap. Thus, more than 52% and 55% of the total incident solar energy contributes to the carrier heating process in Si and GaAs solar cells, respectively [9].

In photovoltaics, hot carriers play a dual role that remains not fully clarified. On the one hand, their excess energy is commonly considered a source of lattice heating, leading to classical thermalization loss [2]. On the other hand, many approaches, including impact ionization [10,11], energy-selective contacts [12,13], incorporation of nanostructures [14,15], multijunction [16,17], and hot carrier solar cells [5], aim to use this excess energy before it is lost. These concepts are theoretically promising, but their practical implementation remains challenging because hot carriers need to be extracted before they cool to the band edge.

Previous studies have shown that the hot carrier effect can directly contribute to the net photoresponse of *p-n* junctions. In particular, below-bandgap infrared radiation induces an HC photocurrent in Ge [4,18], Si [19], and GaAs [20-22] junctions. The observed polarity indicated that HCs move up the potential barrier, in contrast to conventional photogeneration. More recent works have suggested that HC photocurrent may act as an additional intrinsic loss in single-junction solar cells that questions the attainability of the theoretical efficiency limit [6]. However, the formation mechanisms of HC photocurrent under above- and below-bandgap excitation, as well as the effects of temperature and bias voltage, require further clarification.

In this work, the excitation and dynamics of hot carriers are studied in a crystalline GaAs *p-n* junction under pulsed laser excitation at 0.532 and 1.064 μm. These wavelengths represent two different regimes: interband excitation at 0.532 μm, where electron-hole pairs are generated with excess energy, and intraband heating at 1.064 μm, where below-bandgap photons increase the energy of FCs. In addition, the effective hot carrier temperature is determined under different excitation conditions using the voltage-temperature coefficient method.

Earlier works have not directly compared HC formation and transport under interband and intraband excitation in the same device. Using the same structure removes differences between devices and allows the observed effects to be attributed directly to the excitation mechanism. This approach makes it possible to determine whether the opposite-polarity hot carrier current is a universal consequence of carrier heating, to separate its contribution from that of conventional electron-hole pair generation and two-photon absorption, and to evaluate how the effective hot carrier temperature depends on the excitation mechanism and the lattice temperature. This comparison is a further step in assessing whether HC currents are an exploitable resource or an intrinsic pre-thermalization loss in practical single-junction solar cells, because the excitation mechanism determines both the feasibility of energy extraction and the net effect on device output.

In this work, we experimentally compare, for the first time in the same crystalline GaAs *p-n* junction, the formation of hot carrier photocurrent under above-bandgap interband excitation and below-bandgap intraband excitation. This approach makes it possible to determine whether the opposite-polarity hot carrier current is a universal consequence of carrier heating, to separate its contribution from conventional electron-hole pair generation and two-photon absorption, and to evaluate how the effective hot carrier temperature depends on the excitation mechanism, lattice temperature, and bias voltage.

2. Methodology and experimental setup

Crystalline GaAs was chosen for this research because its bandgap is close to the optimal value obtained from the S-Q calculation for maximum single-junction solar cell efficiency [1]. The 2.5×2.5 mm^2 GaAs *p-n* junction test samples consisted of a 5 μm *p*-type layer with a hole concentration of 5×10^{17} cm^{-3}, grown by liquid-phase epitaxy on an *n*-type substrate doped to 3×10^{17} cm^{-3}. Ohmic contacts were thermally evaporated from an Au-Ge-Ni alloy and positioned at the sample's edge to prevent photoresponse at the metal contacts.

The study was carried out at 300 K and 80 K temperatures using time-resolved photocurrent measurements under pulsed laser excitation. The measurement circuit is shown in Fig. 1.

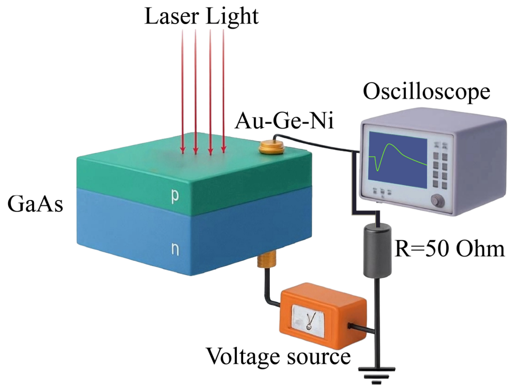

Fig. 1. Schematic of the samples and measurement circuit.

The measurement equipment contains:

- The digital storage oscilloscope DSO6102A by Agilent Technologies (Santa Clara, California, US) was used to record both the photocurrent signal and the laser pulse shapes. The oscilloscope provides registration accuracy of ±2.0% on a vertical scale and the horizontal time-axis of ±15 ps;

- The high-speed optical signal reference detector model 11HSP-FS1 manufactured by Standa Ltd. (Vilnius, Lithuania) provided a measurement of the laser pulse temporal profile;

- The average power of laser radiation was measured with an optical power meter PM400 (Thorlabs Inc., Newton, NJ, USA);

- The custom DC voltage source, capable of providing an adjustable output from 0 to 9 V with a current capability of up to 0.3 A, was used to apply a bias voltage across the GaAs *p-n* junction during the measurements.

Lasers have proven particularly suitable for studying HC phenomena in semiconductors, as they provide monochromatic light, tunable intensity, and ultrafast pulses. The investigation employed a two-wavelength laser system. The Nd: YAG laser operated at a 1.064 µm wavelength with a 18-nanosecond pulse duration, a maximum pulse power of 4.3 MW/cm^2, a beam diameter of 1 mm, and a 50 Hz repetition rate. The second harmonic at 0.532 µm was generated by the same laser, equipped with an LBO nonlinear crystal (NL202; Ekspla Ltd., Vilnius, Lithuania) and a harmonic separator. As a result of these modifications, the laser system produced 7 ns-long pulses, with a maximum pulse power of about 0.5 W/cm^2 and a repetition rate of 50 Hz. The excitation wavelengths of 0.532 µm (2.33 eV) and 1.064 µm (1.17 eV) were selected based on the GaAs bandgap energy, which is approximately 1.42 eV (873 nm) at 300 K and 1.51 eV (820 nm) at 80 K [8]. Above-bandgap excitation (0.532 µm) generates electron-hole pairs with excess energy used for carrier heating. Below-bandgap excitation (1.064 µm) involves free carrier heating and two-photon absorption (TPA).

The 80 K temperature was maintained by custom designed optical cryostat.

3. Results and discussion

Illumination of a GaAs *p-n* junction with laser radiation of below- and above-bandgap photon energies induces carrier transport across the sample, as schematically shown in Fig. 2.

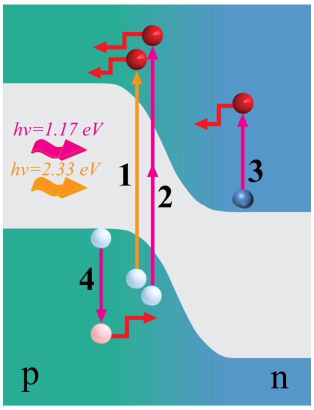

Fig. 2. Schematic illustration of hot carrier transport across an illuminated GaAs *p-n* junction. 1 – hot electron and hole pair creation by light of 2.33 eV photon pulse; 2 – generation of hot electron and hole pair by means of two-photon absorption; 3, 4 – free carrier heating by intraband absorption of 1.17 eV photon pulse. Red stepped arrows demonstrate the hot carrier thermalization and diffusion process.

In Fig. 2, all carrier excitations are governed by HC creation followed by their thermalization. In process 1, interband absorption creates a hot electron and hole pair. Electrons are expected to be heated more strongly than holes because of their substantially lower effective mass [8], allowing them to cross the potential barrier before thermalization. In process 2, two-photon absorption also produces hot electron-hole pairs that exhibit similar charge-transport behavior. Processes 3 and 4 correspond to intraband absorption by electrons and holes, respectively, producing HCs whose diffusion is similar to that in process 1.

Typical experimental temporal shapes of current induced across the *p-n* junction are shown in Fig. 3.

The signal polarities are consistent with the sample connection scheme shown in Fig. 1. Fig. 3a shows the time-resolved short-circuit current (I_{SC}) under below-bandgap illumination. The trace consists of two polarity components. 1) A negative polarity current is associated with HCs diffusing up the potential barrier (red arrows in Fig. 2, processes 2, 3,

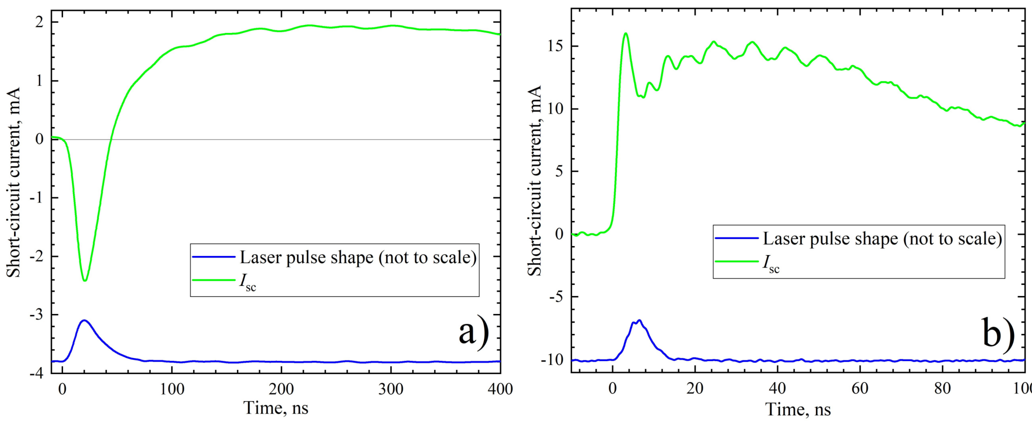

Fig. 3. Typical temporal traces of current across a GaAs *p-n* junction (green line) exposed to pulsed laser light (blue line) of 1.17 eV (a) and 2.33 eV (b) photon energy and intensities of 3.5 and 0.3 MW/cm^2, respectively.

and 4 before their thermalization. The same observation of the output signal was described before in Ref. [20]. 2) A positive component is the photocurrent produced by the generation of electron-hole pairs by TPA (not shown in Fig. 2).

Slightly different behavior is observed in Fig. 3b under the above-bandgap laser illumination of the junction. The positive polarity photocurrent is produced by conventional band-to-band electron-hole generation and their drift in the built-in electric field of the junction. The sharp drop close to the maximum of the laser pulse is caused by HCs generated by the excess photon energy, which diffuse against the built-in electric field (process 1 in Fig. 2). As a result, they give rise to a negative-polarity component of the net signal.

Another fact supporting the presence of the HC current is that it follows the fast laser pulse shape and manifests itself only while the laser pulse is still present. This is a characteristic feature of the HC current behavior [23] since its speed is fundamentally determined by the carrier energy relaxation time, which is on the order of picoseconds in bulk semiconductors [8].

To further elucidate the origin of the currents, the dependence of short-circuit current peak values of the positive and HC components on laser pulse intensity was investigated and is shown in Fig. 4.

Under 0.532 μm excitation, the conventional photocurrent (blue stars), associated with electron-hole pair generation through interband absorption, exhibits a fast rise up to about 6 kW/cm^2, followed by saturation over the remaining power range. The hot carrier current (red stars) is observed at approximately 40 kW/cm^2. A similar manifestation of hot carrier current, emerging after the saturation of the carrier-pair generation-induced photocurrent, has been observed in narrow-bandgap semiconductor *p-n* junctions based on InSb [24] and HgCdTe [25] under CO_2 laser excitation. In contrast to the commonly expected linear dependence, the HC current exhibits superlinear behavior. This deviation is most likely attributable to a generation-induced increase in the free carrier population and may also be influenced by limited accuracy in evaluating the negative peak magnitude superimposed on

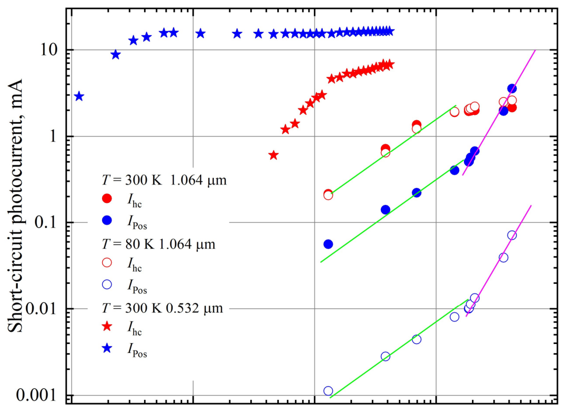

Fig. 4. Short-circuit current dependence of positive (I_{Pos}) and hot carrier (I_{hc}) components on light intensity at two excitation wavelengths. Blue and red stars represent the generation and hot carrier currents, respectively, under 0.532 μm excitation at 300 K. The circles indicate current components under 1.064 μm illumination at 300 K (solid) and 80 K (open): blue – positive current component; red – hot carrier current. The straight lines serve as guides to the eye, corresponding to linear (green) and quadratic (purple) dependences.

the positive pulse of the generation-induced photocurrent (see Fig. 3b). Consequently, above ~0.1 MW/cm^2, the HC current shows the typical tendency of saturation [25].

Under 1.064 μm excitation, the fast negative polarity signal (Fig. 3a) attributed to the HC current initially scales linearly at low intensity (<1 MW/cm^2), since intraband free carrier absorption (Fig. 2, processes 3 and 4) is a first-order process [20]. At higher laser intensities (>2 MW/cm^2), the HC current starts saturating, and the positive photocurrent component goes as the square of the intensity, indicating electron-hole pair generation by means of two-photon absorption [20]. Such a relationship between the two components, namely, the saturation of the first and the rapid increase of the second, suggests that the formation of the hot carrier current is governed predominantly by free carrier absorption rather than by residual energy from two-photon absorption. It is worth noting that the linear dependence of the positive polarity output current at laser intensities below ≈2 MW/cm^2 cannot be attributed to carrier generation, since the photon energy in this regime is lower than the semiconductor bandgap. Instead, this behavior can be explained by a photocapacitive (displacement current) effect arising from partial hot carrier-induced charging (negative signal) and subsequent recharging (positive signal) of the *p-n* junction capacitance under short laser pulses. This process results in a small positive "tail" (recharging) as demonstrated in Ref. [26]. The effect occurs because the pulse duration is only a few times longer than the carrier collection time, which is approximately 5 ns [27].

The intensity dependences of both the HC current and the generation-induced (or positive component) current exhibit similar trends at 300 K and 80 K. The magnitude of the HC current at 80 K is slightly lower than at 300 K up to ≈2 MW/cm^2. This difference can be attributed to a reduced free carrier population (freeze-out effect) and an increased potential barrier height at low temperatures, despite the longer hot carrier energy relaxation time [8]. In the saturation region, however, the HC current at 80 K exceeds that at 300 K. This moderate increase can be explained by an enhanced free carrier population resulting from significantly intensified two-photon absorption above 2 MW/cm^2. The pronounced reduction in the positive component of the current at 80 K can be attributed to the widening of the depletion region, which reduces *p-n* junction capacitance and weakens the photocapacitive response.

The spectral dependence of generation and HC currents in relation to the GaAs absorption coefficient is shown in Fig. 5.

Here, the vertical black line labeled E_g marks the wavelength corresponding to the GaAs bandgap energy. The green line to the left represents interband absorption, while the green line to the longer wavelengths corresponds to intraband absorption. The current values are taken at incident intensities of 0.42 MW/cm^2 and 3.4 MW/cm^2 for 0.532 μm and 1.064 μm excitation, respectively, when the HC currents are saturated and almost independent of intensity. The significantly stronger HC current in the interband region compared to the intraband region can be primarily attributed to the much higher absorption coefficient, despite (i) the substantial difference in excitation intensity, and (ii) the considerably lower photon energy available for carrier heating (0.91 eV in the interband case versus 1.17 eV in the intraband case).

In the case of 0.532 μm excitation, both the generation-induced and HC currents are lower at 80 K due to bandgap widening, which reduces the absorption coefficient and expands the depletion region [8]. Together, these factors hinder hot carrier transport across the potential barrier. The similar absolute decrease of approximately 5–6 mA in both the generation and HC currents suggests a common underlying origin.

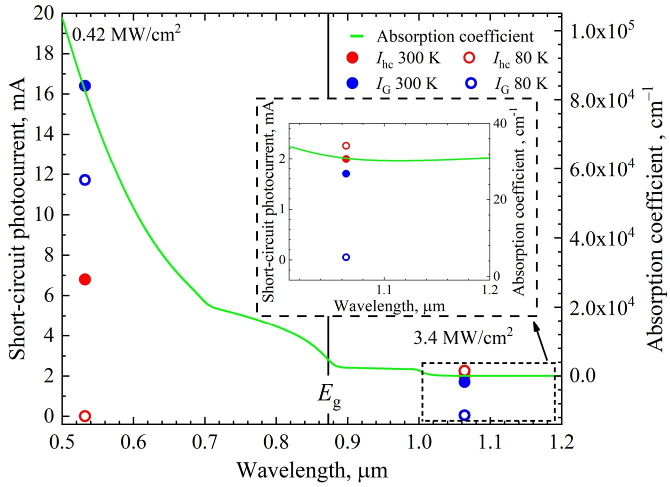

Fig. 5. Short-circuit generation (I_G) and HC (I_{hc}) currents of the GaAs *p-n* junction as a function of excitation wavelength, shown together with the GaAs absorption coefficient (green line). Solid and open symbols correspond to sample temperatures of 300 K and 80 K, respectively. Red symbols indicate the HC current, while blue symbols indicate the generation photocurrent. The absorption coefficient data were taken from [8,28,29]. The insert magnifies the 1.0–1.2 μm wavelength region.

Fig. 6 shows the dependence of the hot carrier currents on the bias voltage. These dependencies enable determination of the "*knee*" voltage, which is subsequently used to evaluate the effective hot carrier temperature (T_{hc}). U_{knee} is selected as the operating point

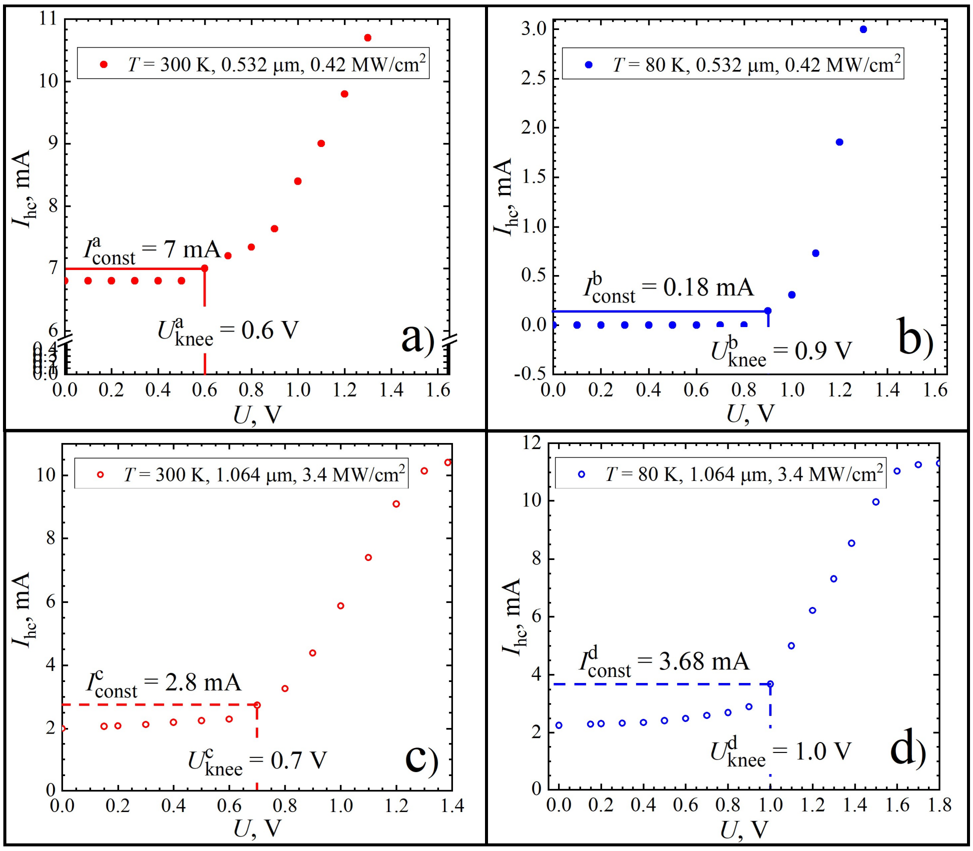

Fig. 6. Dependence of hot carrier current I_{hc} on bias voltage at different temperatures and excitation wavelength.

for effective HC temperature evaluation because, at this bias, the measured response is dominated only by the hot carrier photocurrent, while contributions from dark current and low-bias displacement current under pulsed illumination are negligible.

The diode "*knee*" voltage U_{knee} corresponds to the onset of *p-n* junction opening, at which the hot carrier current begins to increase sharply [30] by transitioning from the displacement current, which flows under reverse and low forward biases, to the transport of hot carriers across the *p-n* junction barrier. Thus, at U_{knee}, the measured response is dominated solely by the hot carrier photocurrent, while contributions from the dark current are negligible.

This transition occurs when the applied voltage sufficiently lowers the junction barrier, enabling hot carriers to cross it [18,30]. The *"knee"* voltages of the HC current are summarized in Table 1.

Table 1. Values of the "*knee*" voltage and corresponding HC current taken from Fig. 6. Index 'x' indicates respective data obtained from a–d subfigures.

Wavelength, μm	0.532		1.064	
Sample temperature, K	300	80	300	80
Intensity, MW/cm^2	0.42		3.4	
U_{knee}^{x}, V	0.6	0.9	0.7	1.0
I_{const}^{x}, mA at U_{knee}^{x}	7	0.18	2.8	3.68

The shift of the "knee" voltage toward higher values at 80 K as compared to 300 K, observed for both excitation wavelengths, reflects the increase in the potential barrier at lower temperature. As a result, a higher forward bias is required to initiate significant hot carrier transport across the junction. At this U_{knee} bias, the measured response is dominated by the hot carrier photocurrent across the barrier, while contributions from the dark current and the low-bias displacement current are negligible [31].

To further elucidate the mechanism of HC photocurrent formation, the effective hot carrier temperature is evaluated using a method developed in earlier works [19,22], based on the temperature dependence of the diode *I-V* characteristics. As the temperature decreases, the dark *I-V* characteristic shifts toward higher voltages because the junction barrier height increases [8,28]. As a result, a well-defined voltage shift is observed at a fixed current, reflecting an increased barrier height. This behavior is characterized by the temperature coefficient [32], a material-specific parameter that specifies the temperature dependence of the diode *I-V* characteristics [33,34]. The temperature coefficient, α_T, is defined as the change in voltage per degree of temperature at a fixed current, $\alpha_T = \Delta U/\Delta T$, where ΔU is the voltage shift, and ΔT is the corresponding temperature change. The value of α_T is determined from the dark *I-V* characteristics measured at 300 K and 80 K at a fixed current I_{const}^{α} = 10.0 mA (Fig. 7a). This constant-current value was selected for several reasons. *First*, a fixed current level was selected within the stable, exponential region of the dark *I-V* characteristics. *Second*, the current is high enough to give a voltage shift with a high signal-to-noise ratio and is low enough to avoid the influence of the series resistance. *Third*, in the current range of approximately 5–15 mA, the calculated α_T values were nearly the same.

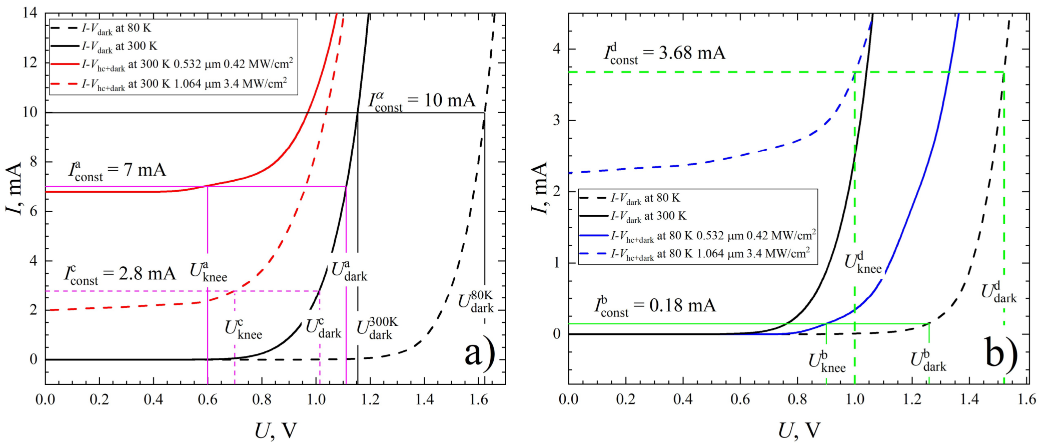

Fig. 7. Dark *I-V* characteristics (*I-V*$_{dark}$) (black lines) and *I-V*$_{hc+dark}$ characteristics of GaAs *p-n* junction measured at 300 K (red lines in a) and 80 K (blue lines in b) temperatures and different excitation wavelengths. Here U^{300K}_{dark} and U^{80K}_{dark} denote the voltages on the *I-V*$_{dark}$ at a fixed dark current of 10 mA at 300 K and 80 K, respectively. $U^{a\text{-}d}_{dark}$ denotes the voltages on the *I-V*$_{dark}$ corresponding to HC current values obtained from Fig. 6 (Table 1) at *"knee"* voltages $U^{a\text{-}d}_{knee}$, respectively.

All values extracted from the graphs of Fig. 7 are summarized in Table 2.

The temperature coefficient was calculated from the shift of the forward voltage between 300 K and 80 K at the fixed value of I^{α}_{const}:

$$\alpha_T = \frac{\Delta U}{\Delta T} = \frac{U^{300K}_{dark} - U^{80K}_{dark}}{T_{300K} - T_{80K}} = \frac{1.155 - 1.625}{300 - 80} = -2.14\,\frac{mV}{K}, \qquad (1)$$

where T_{300K} is the room temperature and T_{80K} is the liquid nitrogen temperature, U^{300K}_{dark} and U^{80K}_{dark} are the voltages of dark *I-V*s at constant current at respective temperatures. The obtained value of α_T agrees well with the range of −(1.88 to 2.30) mV/K reported in the literature for GaAs solar cells [35]. Now, by comparing the *I-V*$_{dark}$ and *I-V*$_{hc+dark}$ characteristics (Fig. 7), the effective carrier temperature can be estimated as:

$$T_{hc} = \frac{\Delta U}{\alpha_T} + T_0 = \frac{U^{x}_{knee} - U^{x}_{dark}}{\alpha_T} + T_0, \qquad (2)$$

where T_0 is the lattice temperature, and index 'x' indicates respective values according to Figs. 6 and 7 (Tables 1 and 2).

Table 2. Parameters for estimating hot carrier effective temperature across different temperatures and excitation wavelengths. Index 'x' indicates respective data obtained from Fig. 7 and a–d subfigures of Fig. 6.

Sample temperature, K	300		80	
I^{α}_{const}, mA	10			
U_{dark}, V	1.155		1.625	
Wavelength, μm	0.532	1.064	0.532	1.064
I^{x}_{const}, mA	7	2.8	0.18	3.68
U^{x}_{dark} at I^{x}_{const}, V	1.11	1.015	1.26	1.52

At 300 K temperature and 0.532 μm illumination of 0.42 MW/cm² intensity, which all are attributed to index 'a' in Eq. (2) and Figs. 6a and 7a, taking the HC voltage value U^{a}_{knee} and U^{a}_{dark} at the same fixed current level I^{a}_{const} = 7 mA, the effective hot carrier temperature is calculated as:

$$T_{hc} = \frac{U^{a}_{knee} - U^{a}_{dark}}{\alpha_T} + T_{300K} = \frac{0.6 - 1.11}{-0.00214} + 300 = 538\ \mathrm{K}\,. \quad (3)$$

Using the same calculation procedure and the data derived from the other *I-V* characteristics shown in Fig. 7, together with the values listed in Tables 1 and 2, the effective hot carrier temperatures were calculated and summarized in Table 3.

Table 3. The calculated effective hot carrier temperatures.

Wavelenght, μm	0.532		1.064	
Intensity, MW/cm²	0.42		3.4	
Sample temperature, K	300	80	300	80
T_{hc}, K	538	248	447	323

It can be seen that the effective HC temperature is more sensitive to changes in lattice temperature under 0.532 μm illumination than under 1.064 μm illumination (538 – 248 = 290 > 124 = 447 – 323). This finding supports the above interpretation, indicating that interband absorption exhibits a more pronounced dependence of hot carrier effect on sample temperature than intraband absorption. It is worth noting that, as shown in Fig. 7b, the hot carrier *I-V*$_{hc+dark}$ characteristic measured at 80 K (blue dashed line) nearly coincides with the dark *I-V*$_{dark}$ characteristic measured at 300 K (black solid line) at the reference current of 3.68 mA. According to Table 3, the corresponding carrier temperature at 80 K is 323 K. This agreement supports the validity of the proposed method for effective carrier temperature evaluation: the same photocurrent can be achieved either by lowering the

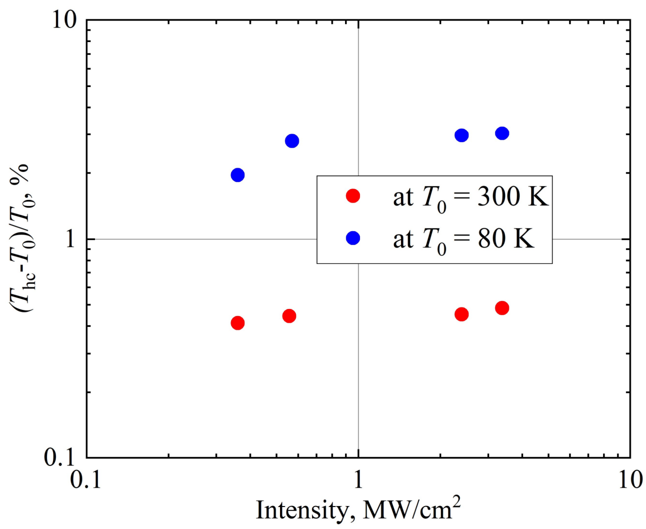

Fig. 8. Dependence of absolute hot carrier temperature T_{hc} on 1.064 μm laser light intensity at 300 K and 80 K temperatures.

potential barrier through an increase in lattice temperature or by increasing the free carrier temperature, thereby enabling carriers to overcome the barrier. This approach of effective HC temperature estimation was applied at various intensities of 1.064 μm illumination at 300 K and 80 K temperatures, and the results are shown in Fig. 8.

It is observed that T_{hc} varies non-proportionally with light intensity at both temperatures, in contrast to the nearly linear HC photocurrent dependence shown in Fig. 4. This sublinearity may arise from several factors. First, at higher carrier energies, energy relaxation becomes more efficient due to enhanced electron-phonon scattering, which is a major energy loss channel in GaAs and other semiconductors [36]. Second, increasing laser intensity also increases the free carrier concentration (e.g., via two-photon absorption), so the absorbed energy is distributed among a larger number of carriers. Third, transport over the barrier itself removes energetic carriers. Finally, a longer carrier energy relaxation time at lower temperatures [8] allows carriers to remain in a non-equilibrium “hot” state for longer, resulting in a higher effective carrier temperature than at 300 K at the same light intensities.

4. Conclusions

Hot carrier transport across a GaAs *p-n* junction under pulsed above-bandgap (0.532 μm) and below-bandgap (1.064 μm) laser excitation was investigated at 300 K and 80 K. The results show that, under interband excitation, the HC photocurrent originates from carriers heated by the excess energy remaining after electron-hole pair generation. Under intraband excitation, the HC current arises from heating of the free carriers. In both cases, the HC photocurrent flows in the direction opposite to that of the electron-hole pair generation-induced photocurrent.

The diode “*knee*” voltage U_{knee}, defined as the forward bias voltage at which the HC current changes from displacement current to hot carrier diffusion across the *p-n* junction barrier, increases with decreasing temperature due to the enhanced potential barrier height. At lower temperatures, the HC displacement (photocapacitive) current is suppressed due to the wider depletion region in the junction.

Analysis of the effective hot carrier temperature, T_{hc} , estimated using the temperature-coefficient model, shows that above-bandgap illumination yields higher T_{hc} values at lower laser intensities than intraband excitation, owing to the much stronger absorption of the radiation. Taking into account the direction of the HC photocurrent, this finding is important for reassessing energy losses in solar cells associated with the direct impact of the hot carrier phenomenon. Under below-bandgap excitation, the rise in effective hot carrier temperature shows a sublinear dependence on light intensity and becomes more pronounced at lower lattice temperatures due to the longer carrier energy relaxation time.

Acknowledgments. The authors are grateful to S. Ašmontas for valuable discussions; to A. Šilėnas for assistance with sample preparation, and to E. Širmulis for help with the installation of the experimental setup.

Disclosures. The authors declare no conflicts of interest.

Author's contributions. Conceptualization, J.G. and O.M.; methodology, J.G., I.Z., and O.M.; experimental investigations, I.Z. and O.M.; writing – original draft preparation, O.M.; writing – review and editing, J.G., I.Z. and O.M.; visualization, J.G, I.Z. and O.M.; supervision, J.G. All authors have read and agreed to the published version of the manuscript.

References

1. Shockley, W., & Queisser, H. J. (1961). Detailed balance limit of efficiency of p-n junction solar cells. *J. Appl. Phys., 32*(3), 510–519.
2. Hirst, L. C., & Ekins-Daukes, N. J. (2011). Fundamental losses in solar cells. *Prog. Photovolt.: Res. Appl., 19*(3), 286–293.
3. Umeno, M., Sugito, Y., Jimbo, T., Hattori, H., & Amemiya, Y. (1977). Hot carrier-voltaic effect in p-n junction and its application to electron emitters and light detectors. *Jpn. J. Appl. Phys., 16*, 283–286.
4. Conwell, E. M. (1967). *High field transport in semiconductors* (Solid State Physics, Suppl. 9). Academic Press.
5. Ross, R. T., & Nozik, A. J. (1982). Efficiency of hot-carrier solar energy converters. *J. Appl. Phys., 53*(5), 3813–3818.
6. Gradauskas, J., Masalskyi, O., Ašmontas, S., Sužiedėlis, A., Rodin, A., & Zharchenko, I. (2024). Hot carrier photocurrent as an intrinsic loss in a single junction solar cell. *Ukr. J. Phys. Opt., 25*(1), 01106–01112.
7. Zhang, Y., Jia, X., Liu, S., Zhang, B., Lin, K., Zhang, J., & Conibeer, G. (2021). A review on thermalization mechanisms and prospect absorber materials for the hot carrier solar cells. *Sol. Energy Mater. Sol. Cells., 225*, 111073.
8. Dargys, A., & Kundrotas, J. (1994). Physical data for gallium arsenide. In *Handbook on the physical properties of Ge, Si, GaAs and InP* (pp. 143–188). Science and Encyclopedia.
9. Masalskyi, O., & Gradauskas, J. (2022). Pre-thermalizational effect of hot carriers on photovoltage formation in a solar cell. *Ukr. J. Phys. Opt., 23*(3), 117–125.
10. Beard, M. C., & Ellingson, R. J. (2008). Multiple exciton generation in semiconductor nanocrystals: Toward efficient solar energy conversion. *Laser Photonics Rev., 2*(5), 377–399.
11. Ikeri, H. I., Onyia, A. I., & Kalu, F. N. (2021). Hot carrier exploitation strategies and model for efficient solar cell applications. *Chalcogenide Let., 18*(11), 745–757.
12. Conibeer, G., Jiang, C.-W., Green, M., Harder, N., & Straub, A. (2003). Selective energy contacts for potential application to hot carrier PV cells. In *Proceedings of the WCPEC-3* (Vol. 3, pp. 2730–2733).
13. Esgandari, M., Barzinjy, A. A., Rostami, A., Rostami, G., & Dolatyari, M. (2022). Solar cells efficiency enhancement using multilevel selective energy contacts (SECs). *Opt. Quantum Electron., 54*, 102.
14. Ašmontas, S., Fedorenko, L., Vlasiuk, V., Gorbanyuk, T., Kostylyov, V., Lytovchenko, V., Gradauskas, J., Sužiedėlis, A., Širmulis, E., Žalys, O., & Masalskyi, O. (2020). Suppression of hot carriers by nanoporous silicon for improved operation of a solar cell. *Ukr. J. Phys. Opt., 21*(4), 207–214.
15. Neupane, K., Kabel, J., Uddin, J., Dubey, R., Ojha, R., Zhang, D., & Yap, Y. K. (2026). Quantum dot solar cells: Background, progress, and perspective. *Micromachines, 17*(4), 474.
16. Raisa, A. T., Sakib, S. N., Hossain, M. J., Rocky, K. A., & Kowsar, A. (2025). Advances in multijunction solar cells: An overview. *Sol. Energy Adv., 5*, 100105.
17. Yamaguchi, M., Dimroth, F., Geisz, J. F., & Ekins-Daukes, N. J. (2021). Multi-junction solar cells paving the way for super high-efficiency. *J. Appl. Phys., 129*(24), 240901.
18. Ašmontas, S., Širmulis, E., & Stonys, S. (1984). Investigation of the photovoltage across germanium p-n junction under pulsed CO_2 laser irradiation. *Lith. J. Phys., 24*, 75–82.
19. Zharchenko, I., Gradauskas, J., Masalskyi, O., & Rodin, A. (2024). Hot carrier photocurrent induced by 0.92 eV photon energy radiation in a Si solar cell. *Opto-Electron. Rev., 32*(2), e15181.
20. Gradauskas, J., Ašmontas, S., Sužiedėlis, A., Šilėnas, A., Vaičikauskas, V., Čerškus, A., Širmulis, E., Žalys, O., & Masalskyi, O. (2020). Influence of hot carrier and thermal components on photovoltage formation across the p-n junction. *Appl. Sci., 10*(21), 7483.
21. Ašmontas, S., Gradauskas, J., Čerškus, A., Sužiedėlis, A., Širmulis, E., & Žalys, O. (2025). Hot carrier transport in solar cells. *Lith. J. Phys., 65*(4), 248–257.
22. Ašmontas, S., Masalskyi, O., Zharchenko, I., Sužiedėlis, A., & Gradauskas, J. (2024). Some aspects of hot carrier photocurrent across GaAs p-n junction. *Inorganics, 12*(6), 174.
23. Ašmontas, S., Gradauskas, J., Sužiedėlis, A., Šilėnas, A., Širmulis, E., Švedas, V., Vaičikauskas, V., & Žalys, O. (2018). Hot carrier impact on photovoltage formation in solar cells. *Appl. Phys. Lett., 113*(7), 071103.
24. Ašmontas, S., Gradauskas, J., Naudjyus, K., & Širmulis, E. (1994). Photoresponse of InSb-based p-n structures during illumination by a CO_2 laser. *Semiconductors, 28*(11), 1089–1091.
25. Ašmontas, S., Gradauskas, J., Seliuta, D., Sužiedėlis, A., Širmulis, E., Valušis, G., & Tetyorkin, V. V. (2002). CO_2 laser induced hot carrier photoeffect in HgCdTe. *Materials Science Forum, 384–385*, 147–150.
26. Ašmontas, S., Gradauskas, J., Sužiedėlis, A., Širmulis, E., & Urbelis, A. (2006). Hot carrier photocapacitive effect. In *Optical materials and applications* (Proceedings of SPIE, Vol. 5946, 594619).

27. Levinshtein, M. E., & Rumyantsev, S. L. (1996). Gallium arsenide (GaAs). In M. Levinshtein, S. Rumyantsev, & M. Shur (Eds.), *Handbook series on semiconductor parameters: Si, Ge, C (diamond), GaAs, GaP, GaSb, InAs, InP, InSb* (Vol. 1, pp. 77–103). World Scientific.
28. Sze, S. M. (1969). *Physics of semiconductor devices*. Wiley.
29. Adachi, S. (1989). Optical dispersion relations for GaP, GaAs, GaSb, InP, InAs, InSb, $Al_xGa_{1-x}As$, and $In_{1-x}Ga_xAs_yP_{1-y}$. *J. Appl. Phys., 66*(12), 6030–6040.
30. Ašmontas, S., Gradauskas, J., Seliuta, D., Sužiedėlis, A., Šilėnas, A., & Valušis, G. (1997). GaAs/AlGaAs heterojunction: A promising detector for infrared radiation. In *Proceedings of the 5th European Gallium Arsenide and Related III–V Compounds Applications Symposium* (pp. 345–348).
31. Gradauskas, J., & Ašmontas, S. (2021). Hot carrier photocurrent through MOS structure. *Appl. Sci., 11*(16), 7211.
32. Schaffner, J. S., & Shea, R. F. (1955). The variation of the forward characteristics of junction diodes with temperature. *Proceedings of the IRE, 43*(1), 101–107.
33. Shayan, S., Matloub, S., & Rostami, A. (2021). Efficiency enhancement in a single bandgap silicon solar cell considering hot-carrier extraction using selective energy contacts. *Opt. Express, 29*(4), 5068–5080.
34. Green, M. A., Emery, K., & Blakers, A. W. (1982). Silicon solar cells with reduced temperature sensitivity. *Electron. Lett., 18*(2), 97–98.
35. Singh, P., & Ravindra, N. M. (2012). Temperature dependence of solar cell performance – An analysis. *Sol. Energy Mater. Sol. Cells., 101*, 36–45.
36. Bernardi, M., Vigil-Fowler, D., Ong, C. S., Neaton, J. B., & Louie, S. G. (2015). Ab initio study of hot electrons in GaAs. *Proceedings of the National Academy of Sciences of the United States of America, 112*(17), 5291–5296.

Masalskyi, O., Zharchenko, I., Gradauskas, J. (2026). Peculiarities of Hot Carrier Transport across GaAs *p-n* Junctions under Interband and Intraband Excitation. *Ukrainian Journal of Physical Optics*, *27*(3), 03225 – 03237. doi: 0.3116/16091833/Ukr.J.Phys.Opt.2026. 03225

Анотація. *У фотовольтаїці роль гарячих носіїв заряду досі неоднозначна. Позитивний вплив гарячих носіїв пов'язують із можливістю створення високоефективних сонячних елементів, тоді як їх негативний вплив розглядають як джерело втрат енергії через термалізацію. У цій роботі досліджено формування фотоструму гарячих носіїв у кристалічному p-n переході GaAs, перспективному для застосування у високоефективних сонячних елементах, за імпульсного лазерного збудження на довжинах хвиль 0,532 і 1,064 μм. Вимірювання часової залежності фотоструму проводилися при температурах 300 K та 80 K. Фотострум гарячих носіїв із полярністю, протилежною до струму генерації електронно-діркових пар, виникає як за надзонного, так і за підзонного збудження. Однак за надзонного збудження він є більш вираженим через значно сильніше міжзонне поглинання. Показано, що ефективна температура гарячих носіїв, оцінена за допомогою моделі температурного коефіцієнта, ефективніше підвищується при опроміненні фотонами з енергією вищою за ширину забороненої зони та при нижчій температурі зразка.*

Ключові слова: *GaAs, гарячі носії, температурний коефіцієнт, ефективна температура носіїв, p-n перехід, лазери*